

Multiferroic Rhodium Clusters

Lei Ma,¹ Ramiro Moro,² John Bowlan,¹ Andrei Kirilyuk,³ and Walt A. de Heer¹

¹*School of Physics, Georgia Institute of Technology, Atlanta, Georgia 30332, USA*

²*Cameron University, Lawton, Oklahoma 73505, USA*

³*Radboud University Nijmegen, Institute for Molecules and Materials, 6525 AJ Nijmegen, The Netherlands*

(Received 22 January 2014; published 6 October 2014; corrected 7 January 2015)

Simultaneous magnetic and electric deflection measurements of rhodium clusters (Rh_N , $6 \leq N \leq 40$) reveal ferromagnetism and ferroelectricity at low temperatures, while neither property exists in the bulk metal. Temperature-independent magnetic moments (up to $1\mu_B$ per atom) are observed, and superparamagnetic blocking temperatures up to 20 K. Ferroelectric dipole moments on the order of $1D$ with transition temperatures up to 30 K are observed. Ferromagnetism and ferroelectricity coexist in rhodium clusters in the measured size range, with size-dependent variations in the transition temperatures that tend to be anticorrelated in the range $n = 6$ –25. Both effects diminish with size and essentially vanish at $N = 40$. The ferroelectric properties suggest a Jahn-Teller ground state. These experiments represent the first example of multiferroic behavior in pure metal clusters.

DOI: [10.1103/PhysRevLett.113.157203](https://doi.org/10.1103/PhysRevLett.113.157203)

PACS numbers: 75.85.+t, 73.22.-f, 75.50.Cc, 77.80.-e

The $4d$ and $5d$ transition-metal clusters are particularly interesting because magnetism can be stabilized on the nanoscale, despite the nonmagnetic character of their bulk materials. Rhodium stands out because it is located at the center of the periodic table with an unfilled $4d$ shell, which produces rich physical and chemical properties. Rhodium clusters have been intensively studied by using theoretical methods [1–6] to understand their catalytic properties and the emergence of the electronic and magnetic properties [7–10]. Small rhodium clusters were found to possess magnetic moments [11,12] on the order of one Bohr magneton ($1\mu_B$) per atom, making this the only $4d$ element with magnetic order at the nanoscale and with Mn [13] the only known elements that are magnetic at nanoscale but not in the bulk.

Prior electric polarizability measurements of rhodium clusters, performed at $T = 49$ K [14] revealed electric dipole moments in Rh_7 and Rh_{10} . Because of its temperature dependence, Rh_{10} was classified as paraelectric [14] (i.e., a ferroelectric above its transition temperature). Since multiferroics are materials that simultaneously exhibit more than one primary ferroic order [15–17], the earlier experiments suggest that small rhodium clusters might be multiferroic at low temperatures. Coexistence of ferroelectric and ferromagnetic order had been predicted in tantalum clusters [18]. While tantalum clusters are indeed ferroelectric at low temperature, our investigations found odd- N Ta_N clusters to be paramagnetic and even- N clusters to be nonmagnetic at all temperatures. These considerations motivated the search for multiferroic order in Rh_N presented here.

Our cryogenic molecular beam apparatus is uniquely suited for this task, because magnetic and electric deflection measurements can be performed under identical

conditions. The clusters are produced in a cryogenic pulsed laser vaporization cluster source, and they are detected in a high-resolution, position-sensitive time-of-flight mass spectrometer, where the mass and deflection of the clusters in the beam are individually measured and recorded. Specifically (for details, see, for example, [19,20]), a beam of clusters is ejected from a well-thermalized helium-filled chamber in the source, whose temperature T can be accurately adjusted from $T = 20$ K to $T = 300$ K. The beam is collimated to 0.3 mm. After passing through an inhomogeneous magnetic field (using a Stern-Gerlach magnet) and an inhomogeneous electric field (two-wire field), the clusters arrive at the mass spectrometer 2 m away, where they are (singly) ionized by using a pulsed excimer laser before entering the mass spectrometer. The deflections can be measured with sensitivities of up to a few microns.

While individual (isolated) clusters in the beam do not have a defined temperature (because the internal state of each isolated cluster in the beam is fixed), the ensemble of clusters in the beam represents a “frozen” canonical ensemble reflecting the source temperature. Therefore, the average properties of the ensemble of clusters in the beam are properly described in terms of the source temperature and applied fields [21,22].

Figure 1 shows the magnetic deflection profile for several representative rhodium clusters at $T = 20$ K and $T = 40$ K. Several clusters (for example, Rh_{18} ; see also Supplemental Material [23]) show a deflection profile (red, lighter) that is slightly broadened compared with the 0 field peak (blue, darker), characteristic of ferromagnetic clusters. Others (for example, Rh_7 , Rh_8 , and Rh_{17} shown in Fig. 1) show bimodal deflections, consisting of a central peak superimposed on a broad plateau. The plateau diminishes with increasing temperature, while the central peak increases.

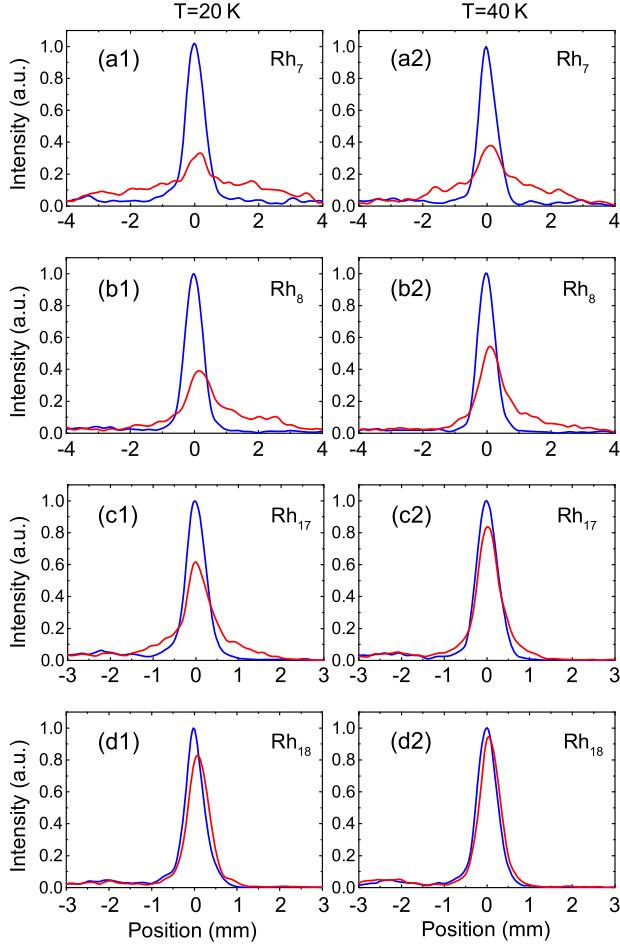


FIG. 1 (color online). Magnetic deflection profiles of four representative rhodium clusters at $T = 20$ K and $T = 40$ K, without (blue, darker) and with (red, lighter) a magnetic field (0.93 T). Notice that, at 20 K, the deflected profiles of Rh_7 (a1), Rh_8 (b1), and Rh_{17} (c1) show typical locked moment deflections, resulting in broad plateaus with wings that extend in the positive and negative direction. The relatively narrow, slightly deflected central peak is on the top of the plateau. Rh_{18} (d1) has a simple deflection peak, typical of (unlocked) ferromagnetic behavior. At 40 K, the wings for Rh_7 (a2), Rh_8 (b2), and Rh_{17} (c2) are significantly reduced (with a corresponding increase in the peak) characteristic of the “unlocking” of the magnetic moment.

The magnetization M of a cluster is found from its deflection d by $d = K_M(MI/mv^2)$, where I is the magnet current, m is the cluster mass, v is the cluster velocity, and K_M is a constant. References [21,22] explicitly demonstrate that the ensemble average magnetization of ferromagnetic clusters, whose magnetic moment (i.e., total spin) is coupled to the rotations (not to a cluster axis), follows the Langevin equation (at least in the extremes of low and high magnetic fields). Consequently, for Rh_N

$$(k_B T \gg \mu N B), \quad (1)$$

$$(k_B T \ll \mu N B), \quad (2)$$

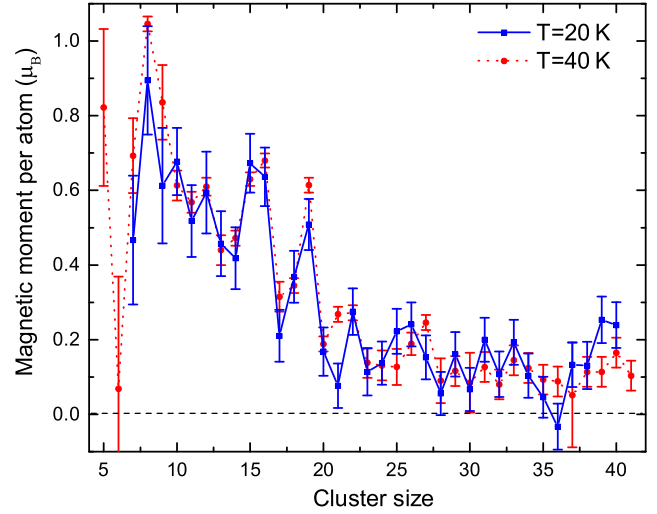


FIG. 2 (color online). Magnetic moments per atom of Rh_N measured at $T = 20$ K (blue line) and $T = 40$ K (red dashed line). These values are consistent with those measured at a higher temperature (from 60 to 300 K) [11,12], showing that the magnetic moment per atom, that is determined from the deflection of the central peak, is temperature independent.

where μ is the magnetic moment per atom and M is the magnetization.

The magnetic moments derived from the central peak position are shown in Fig. 2. Note their temperature independence. On the other hand, if the spin is strongly coupled to an axis in the cluster (i.e., locked), then the magnetic moment distributions are significantly modified, resulting in a broad flat distribution extending from $M = -\mu N$ to $+\mu N$ (see, for example, [20]). This “locked moment” behavior [24], first observed in rare earth clusters [25], is also clearly seen in several Rh clusters as shown in Fig. 1. The transition from Langevin-like behavior to locked behavior is seen in several clusters that show a relatively sharp peak (due to unlocked moments) superimposed on a broad plateau (due to locked moments) and the central peak increases in intensity with increasing temperature. The transition from locked to free motion with increasing temperature is well known in superparamagnets [25] and molecular magnets [26].

The total energy E of an individual cluster in a molecular beam is fixed (for a discussion of their ferromagnetic properties in a molecular beam, see Ref. [21]). At cryogenic temperatures, clusters are (typically) in the ground vibrational states (due to the large Debye temperature) and in highly excited rotational states (due to the large moment of inertia I). Therefore, in the simplest approximation, we assume that the uncoupling of the spin from the cluster axis (unlocking) at cryogenic temperatures occurs when the rotational energy exceeds a critical (cluster-dependent) value $E_{LM}(N)$ (corresponding to a transition from Hund’s coupling case a to coupling case b in paramagnetic molecules [23]). For slightly asymmetric clusters, the

density of rotational states is approximately constant: $n_{\text{rot}} = 2I/\hbar^2$ [23]. Consequently, the probability that a specific cluster will emerge from the source with (rotational) energy below $E_{LM}(N)$ is given by

$$S_{LM}(N, T) = 1 - e^{(E_{LM}(N)/k_B T)} = 1 - e^{(-T_{LM}(N)/T)}. \quad (3)$$

Since both the locked and unlocked components are clearly distinguished, this allows the transition temperature $T_{LM}(N) = E_{LM}(N)/k_B$ to be determined.

We next turn to the electric deflections. Electric deflection beam profiles of several clusters at $T = 20$ and 40 K are shown in Fig. 3. The per-atom polarizabilities are determined from the average electric deflections \bar{x} (Fig. 4)

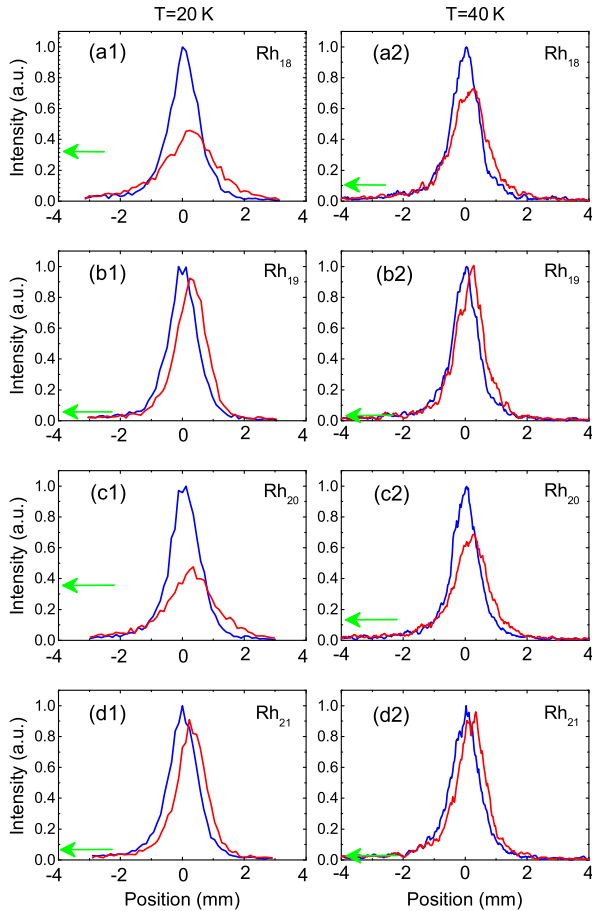


FIG. 3 (color online). Electric deflection profiles of four representative rhodium clusters at $T = 20$ K (left column) and $T = 40$ K (right column), without (blue) and with (red) an electric field $E = 80$ kV/cm. Notice that Rh_{19} (b1) and Rh_{21} (d1) exhibit normal metallic polarizabilities resulting in uniform deflections, while Rh_{18} (a1) and Rh_{20} (c1) show ferroelectric behavior [18,19], with significant intensity loss and broadened peaks. The green arrows show the intensity loss, i.e., the ferroelectric fraction, corresponding to the fraction of the clusters that are deflected beyond the detector window. The ferroelectric fractions at $T = 40$ K are smaller than at $T = 20$ K, consistent with Eq. (5).

by using $\bar{x} = K(\alpha V^2/mv^2)$, where m is the cluster mass, V is the deflection plate voltage, and K is constant. In the metallic sphere picture, the polarizability α_N of a metallic cluster can be written as

$$\alpha_N = 4\pi\epsilon_0 R_N^3 = 4\pi\epsilon_0 (N^{-1/3} R_0 + d_N)^3, \quad (4)$$

where R_N is the screening radius, R_0 is the atomic radius in the bulk, and d_N is the “spillover” (typically on the order of 1 Å) indicating the distance beyond the classical radius where external electric fields are screened [27]. This first-order approximation for metal cluster polarizabilities applies reasonably well even to nonspherical clusters [27–30]. Size-dependent deviations from Eq. (4) (typically on the order of 10%) are observed in various clusters have been ascribed to electronic structure and shapes [14]. The metallic screening picture describes the response of metal clusters to electric fields in most cases. For Rh_N , $d \approx 0.5$ Å, see Fig. 4.

However, note in Fig. 3 that the integrated intensity of the deflected beam (i.e., the area of the electric deflected peaks) is reduced compared with the undeflected beam. This behavior is a well-known signature of ferroelectric clusters [18] for which the electric deflections are bimodal. Specifically, the reduction results from relatively large electric dipole moments causing clusters to deflect well beyond the detector window. For example, for Rh_{18} the intensity is depleted by about 0.28. Hence, the deflections

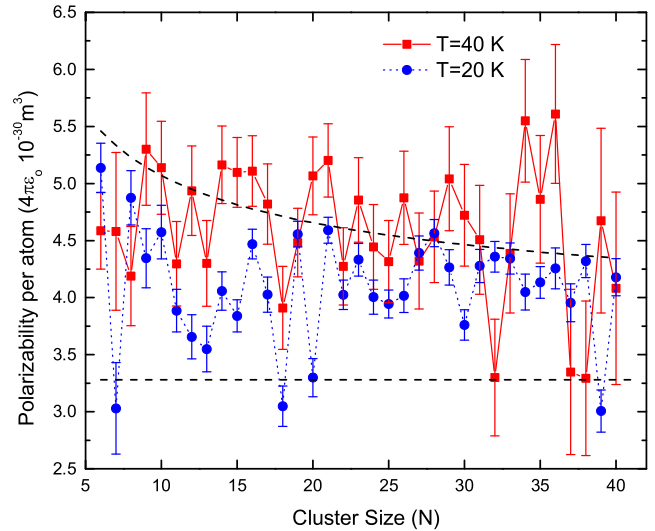


FIG. 4 (color online). Electric polarizabilities per atom of rhodium clusters measured at $T = 20$ K (blue line) and $T = 40$ K (red dashed line), as determined from the electric deflection profiles (Fig. 3) using Gaussian fits. The metallic sphere value is $3.28 \times 10^{-30} \text{ m}^3$ ($4\pi\epsilon_0$), black dashed line. The top black dashed curve represents Eq. (4) with $d_N = 0.5$ Å [14,31], approximating the 40 K data reasonably well. The 20 K measurements show generally reduced values (yet still greater than the metallic sphere value) and size-dependent fluctuations as also seen in Ref. [14].

consist of a normal component with polarizabilities that are in the expected metal cluster range as shown above (Fig. 4) and a ferroelectric component consisting of clusters with large electric dipole moments to produce an essentially single-sided “tail” that ranges far beyond the detector window. The values of the dipole moments are not of importance here (they are found to be on the order of $1D$; see Supplemental Material [23]). The ferroelectric fraction S_G (i.e., the magnitude of the ferroelectric component) is temperature- and cluster-size-dependent, diminishing and ultimately vanishing at high temperature. As seen in Fig. 2 for Rh_{18} , $S_G(N=18, T=20\text{ K})=0.28$, while $S_G(N=18, T=40\text{ K})=0.10$. The values for other clusters are given in Supplemental Material [23]. For all clusters, $S_G=0$ at $T=300\text{ K}$ [14] (see Supplemental Material [23]).

The polarizabilities (of the normal components) of clusters with large S_G (i.e., $N=7, 18$, and 20 , at $T=20\text{ K}$) are systematically somewhat smaller compared with those with small S_G , while the deflected peaks are slightly broader. These variations diminish with increasing temperature, and already at $T=40\text{ K}$ (Fig. 3) the polarizabilities of most clusters are close to their high temperature values (see Supplemental Material [23]), where the ferroelectric fractions are vanishingly small.

Note that the behavior observed here is distinct from that observed for clusters with large permanent electric dipole moments, which do not exhibit bimodal deflections. For polar clusters the deflected peaks exhibit essentially symmetric broadening (due to the random initial orientation of the dipoles in the deflecting fields [24,32–34]) superimposed on a uniform deflection (due to the usual cluster polarizability). More importantly, the dipoles persist at all temperatures, and there is no transition to normal metallic screening behavior [Eq. (4)].

In order to quantify the ferroelectric fraction, we follow the simple picture outlined in Ref. [18]. As for the magnetic transition above, we assume that the transition from ferroelectric to metallic behavior involves an excitation of a single harmonic mode in the cluster, with a characteristic energy $\hbar\omega_G$. If in a specific cluster the excitation n of this mode exceeds E_{\min} so that $n = E_{\min}/\hbar\omega_G$, then the cluster will exhibit normal properties; below this energy, it is ferroelectric. Consequently, the fraction of clusters in the ferroelectric state in the beam is

$$S_G(N, T) = 1 - e^{-[T_G(N)/T]}, \quad (5)$$

where $T_G(N) = E_{\min}/k_B$ is the transition temperature for a cluster with size N .

The transition temperatures determined from Eq. (5) for these clusters is shown in Fig. 5 (shown in red). Note that the temperatures are below 10 K. [Figure 5 also reports the magnetic transition temperatures determined from Eq. (3) (blue).]

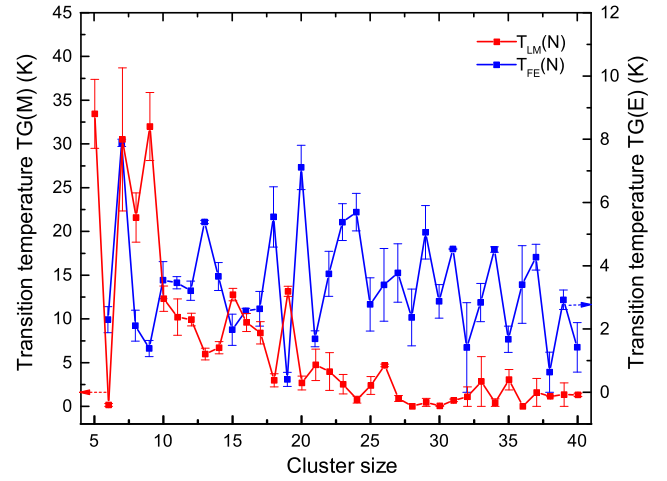


FIG. 5 (color online). Transition temperatures from locked magnetic moments to unlocked moments $T_{LM}(N)$ (blue) and the ferroelectric transition temperature $T_{FE}(N)$ (red, values multiplied by 3), using Eqs. (3) and (5), respectively. Note that size-dependent variations in $T_{LM}(N)$ and $T_{FE}(N)$ tend to be anticorrelated.

Note that characteristic vibrational energies are on the order of the Debye temperature (i.e., 350 K for Rh) and that characteristic electronic energies are on the order of E_F/N (corresponding to at least hundreds of degrees), where E_F is the Fermi energy (see, for example, [35]). Consequently, the ferroelectric transition is not mediated by a (pure) electronic excitation or a (pure) vibration in the cluster. However, it may be a vibronic mode that is a combination of the two, as, for example, in the Jahn-Teller effect. Symmetry-breaking Jahn-Teller distortions can cause ferroelectricity [36] and also typically give rise to low energy vibronic modes [37]. In general, excitations of these modes restore the original symmetry and thereby cause the ferroelectric dipole moment to vanish. Hence, the ferroelectric properties may be caused by the Jahn-Teller effect.

While the generic discussion above is probably correct, the exact mechanism by which the electric dipole moments are created is clearly not explained. We emphasize that asymmetry (or the lack of inversion symmetry) itself is not sufficient to cause *significant* electric dipole moments in metal clusters as explicitly experimentally demonstrated in Ref. [30]. In prior work, we argued that electronic correlations, probably related to superconducting pairing interactions, combined with Jahn-Teller distortions play a role in the ferroelectric behavior of vanadium, tantalum, and niobium clusters. It was argued that correlations can cause the electronic structure to become rigid, thereby reducing electronic screening. In the present case, electron pairing is probably not the cause, since there is no evidence for an even-odd effect. Moreover, the superconducting transition in Rh is exceptionally small (0.36 mK) [38], and, furthermore, ferromagnetism generally suppresses electron pairing.

As can be seen in Fig. 5, cluster-size-dependent variations in the transition temperatures $T_{LM}(N)$ and $T_{FE}(N)$ tend to be anticorrelated. Even if the harmonic approximation used to extract these transition temperatures is not precise, it is fairly certain that the overall trends will be maintained in a more accurate description. In any case, this inverse relationship implies that the magnitude of the vibronic coupling causing ferroelectric effect is inversely related to the magnitude of the spin-orbit coupling that ultimately causes the magnetic anisotropy (and the coupling of the spin to cluster). We are not aware if a related competition between ferroic orders occurs in other multiferroic systems. It is also particularly interesting to note that both the magnetic moment and the ferroelectric diminish uniformly with increasing size and essentially vanish for $N = 40$.

In conclusion, we have presented the first example of multiferroic behavior in metal clusters. The fact that it is observed in rhodium clusters is even more striking, since this metal is neither ferromagnetic nor ferroelectric in the bulk. Yet these properties emerge simultaneously in small clusters and vanish more or less uniformly with increasing size. From a broader perspective, the emergence of ferroelectricity in small metal clusters appears to be mediated by very low energy excitations, possibly involving a single vibronic mode that is associated with a broken symmetry ground state.

The authors acknowledge enlightening discussions with Cristian Batista, Jorge Hirsch, and Vitaly Kresin. This work was supported by the NSF under Grants No. DMR-1006352 and No. DMR-1308835.

-
- [1] B. V. Reddy, S. N. Khanna, and B. I. Dunlap, *Phys. Rev. Lett.* **70**, 3323 (1993).
- [2] J. Yang, F. Toigo, and W. Kelin, *Phys. Rev. B* **50**, 7915 (1994).
- [3] F. Aguilera-Granja, J. L. Rodríguez Lopez, K. Michaelian, E. O. Berlanga-Ramírez, and A. Vega, *Phys. Rev. B* **66**, 224410 (2002).
- [4] Y. Bae, H. Osanai, V. Kumar, and Y. Kawazoe, *Phys. Rev. B* **70**, 195413 (2004).
- [5] F. Aguilera-Granja, J. M. Montejano-Carrizalez, and R. A. Guirado-López, *Phys. Rev. B* **73**, 115422 (2006).
- [6] M. A. Mora, M. A. Mora-Ramírez, and Manuel F. Rubio-Arroyo, *Int. J. Quantum Chem.* **110**, 2541 (2010).
- [7] C. Chien, E. Blaisten-Barojas, and M. R. Pederson, *Phys. Rev. A* **58**, 2196 (1998).
- [8] P. Parida, A. Kundu, and S. K. Pati, *J. Cluster Sci.* **20**, 355 (2009).
- [9] V. Sessi, K. Kuhnke, J. Zhang, J. Honolka, and K. Kern, *Phys. Rev. B* **82**, 184413 (2010).
- [10] H. K. Yuan, H. Chen, A. L. Kuang, B. Wu, and J. Z. Wang, *J. Phys. Chem. A* **116**, 11673 (2012).
- [11] A. J. Cox, J. G. Louderback, and L. A. Bloomfield, *Phys. Rev. Lett.* **71**, 923 (1993).
- [12] A. J. Cox, J. G. Louderback, S. E. Apsel, and L. A. Bloomfield, *Phys. Rev. B* **49**, 12295 (1994).
- [13] M. B. Knickelbein, *Phys. Rev. Lett.* **186**, 5255 (2001).
- [14] M. K. Beyer and M. B. Knickelbein, *J. Chem. Phys.* **126**, 104301 (2007).
- [15] *Magnetolectric Interaction Phenomena in Crystals*, edited by A. J. Freeman and H. Schmid (Gordon and Breach, New York, 1995).
- [16] R. Ramesh and N. A. Spaldin, *Nat. Mater.* **6**, 21 (2007).
- [17] L. W. Martin and R. Ramesh, *Acta Mater.* **60**, 2449 (2012).
- [18] W. Fa, C. Luo, and J. Dong, *J. Chem. Phys.* **125**, 114305 (2006).
- [19] R. Moro, X. Xu, S. Yin, and W. A. de Heer, *Science* **300**, 1265 (2003).
- [20] X. Xu, S. Yin, R. Moro, A. Liang, J. Bowlan, and W. A. de Heer, *Phys. Rev. Lett.* **107**, 057203 (2011).
- [21] X. Xu, S. Yin, R. Moro, and W. A. de Heer, *Phys. Rev. Lett.* **95**, 237209 (2005).
- [22] X. Xu, S. Yin, R. Moro, and W. A. de Heer, *Phys. Rev. B* **78**, 054430 (2008).
- [23] See Supplemental Material at <http://link.aps.org/supplemental/10.1103/PhysRevLett.113.157203> contains additional electric and magnetic deflection profiles of other rhodium clusters, a figure with ferroelectric fractions for different sizes and two temperatures, a figure that compares the ferroelectric fraction and magnetic moments and a table with the ferroelectric fractions and the dipole measure directly from the tail of the profiles.
- [24] G. F. Bertsch and K. Yabana, *Phys. Rev. A* **49**, 1930 (1994).
- [25] A. J. Cox, D. C. Douglass, J. G. Louderback, A. M. Spencer, and L. A. Bloomfield, *Z. Phys. D* **26**, 319 (1993).
- [26] D. C. Douglass, A. J. Cox, J. P. Bucher, and L. A. Bloomfield, *Phys. Rev. B* **47**, 12874 (1993).
- [27] W. A. de Heer, *Rev. Mod. Phys.* **65**, 611 (1993).
- [28] W. D. Knight, K. Clemenger, W. A. de Heer, and W. Saunders, *Phys. Rev. B* **31**, 2539 (1985).
- [29] G. Tikhonov, V. Kasperovich, K. Wong, and V. V. Kresin, *Phys. Rev. A* **64**, 063202 (2001).
- [30] J. Bowlan, A. Liang, and W. A. de Heer, *Phys. Rev. Lett.* **106**, 043401 (2011).
- [31] J. P. Perdew, *Phys. Rev. B* **37**, 6175 (1988).
- [32] P. Dugourd, I. Compagnon, F. Lepine, R. Antoine, D. Rayane, and M. Broyer, *Chem. Phys. Lett.* **336**, 511 (2001).
- [33] P. Dugourd, R. Antoine, M. Abd El Rahim, D. Rayan, M. Broyer, and F. Calvo, *Chem. Phys. Lett.* **423**, 13 (2006).
- [34] S. Schäfer, S. Heiles, J. A. Becker, and R. Schäfer, *J. Chem. Phys.* **129**, 044304 (2008).
- [35] D. Gatteschi and R. Sessoli, *Angew. Chem., Int. Ed.* **42**, 268 (2003).
- [36] P. W. Anderson and E. I. Blount, *Phys. Rev. Lett.* **14**, 217 (1965).
- [37] G. Herzberg, *Molecular Spectra and Molecular Structure* (Krieger, Malabar, FL, 1989).
- [38] C. Buchal, F. Pobell, R. H. Mueller, M. Kubota, and J. R. Owers-Bradley, *Phys. Rev. Lett.* **50**, 64 (1983); C. H. Townes and A. L. Schawlow, *Microwave Spectroscopy* (McGraw-Hill, New York, 1955).